RSC Advances

Fabrication of TiO2@ZnAl-layered double hydroxide based anode material for dye-sensitized solar cell

Journal:	*RSC Advances*
Manuscript ID	RA-ART-11-2015-023384.R1
Article Type:	Paper
Date Submitted by the Author:	01-Jan-2016
Complete List of Authors:	Jafari Foruzin, Leila; Azarbaijan Shahid Madani University, Chemistry Rezvani, Zolfaghar; Azarbaijan Shahid Madani University, Chemistry Nejati, Kamellia; Payame Noor University, P.O. BOX 19395-3697
Subject area & keyword:	Solar energy < Energy

RSC Advances

ARTICLE

Fabrication of TiO_2@ZnAl-layered double hydroxide based anode material for dye-sensitized solar cell

Received 00th January 20xx,
Accepted 00th January 20xx

DOI: 10.1039/x0xx00000x

www.rsc.org/

Leila Jafari Foruzin[a], Zolfagfhar Rezvani[a]* and Kamellia Nejati [b]

Abstract

The TiO_2@ZnAl-layered double hydroxide nanocomposite was prepared by the co-precipitation method; then, the product was calcined in order to obtain the TiO_2@MMO nanocomposite. The products were characterized using scanning electron microscopy (SEM), X-ray diffraction (XRD), thermogravimetric analysis (TGA), Fourier transmission infrared spectroscopy (FT-IR) technique, and UV– vis diffuse reflectance spectra (DRS). The resulting material was employed as a photoanode whose high conversion efficiency, η , in dye-sensitized solar cells (DSSCs) in comparison with ZnAl- layered double hydroxide was attributed to the enlargement of the surface area by the nanosize plates and increased adsorption of the dye by TiO_2, which was placed on the nanoplate. It was found that decrease in the thickness of the film (4.72 μm) led to increase in the open-circuit voltage (V_{OC}), decrease in the recombination rate, and improvement in the efficiency of the dye sensitized solar cell.

Keywords: Dye-sensitized Solar cell; TiO2; Mixed metal oxide; Nanocomposite

[a] Department of Chemistry, Faculty of Basic Sciences, Azarbaijan Shahid Madani University, Tabriz, Iran, Fax: +98 412 432 7541; Tel: +98 413 432 7541; E-mail: zrezvani@azaruniv.ac.ir
[b] Department of Chemistry, Payame Noor University, P.O. BOX 19395-3697, Tehran, Iran

1. Introduction

Among the different technologies, solar energy conversion has unique potential to meet the energy demands. The solar energy which reaches the earth in 1 h is almost equivalent to the current global annual energy consumption. In order to replace the use of fossil fuels and petroleum with other clean forms of energy, conversion of sunlight energy into electrical energy seems to be one of the most promising solutions for the energy tension problem. [1, 2] Dye-sensitized solar cells (DSSCs) is an emerging solar technology that is considered to be an alternative to the conventional first and second generation photovoltaic devices [3].

Since publication of the initial paper by Grätzel et al. on dye sensitized solar cells, there have been several investigations due to their particular features, such as its low-cost fabrication with high solar energy-to-electrical energy conversion efficiencies.[4-10]

A typical DSSC is composed of a dye-sensitized TiO_2 photoanode deposited on a FTO (SnO_2:F) transparent conductive glass as the working electrode, a redox electrolyte normally containing I^-/I_3^- species, and a Pt counter electrode.

In fact, for improving the conversion efficiency and being economically in industrial mass production, DSSCs are constantly asking for more and more efficient (metal-)organic dyes, oxidic semiconductors, metallic and polymeric counter electrodes , liquid and quasi-solid electrolytes, hole-transporting and sealing materials.[11] Recently, SnO_2 photoanodes [12] and flexible TiO_2 photoanodes [13] were used in DSSC. The photoanode of a DSSC, which is made of semiconductor nanostructure materials, plays an important role in the performance of the solar cell.

However, it still remains a great challenge to improve DSSCs that are both low-cost and efficient enough to generate energy at a price that is competitive with fossil fuel.[14]

One of the novel materials for potential application in solar energy conversion is layered double hydroxides (LDHs) due to their high specific surface area, tuneable composition, simple synthesis methods, low cost, and stability. LDHs, as a family of layered anionic materials representing an important class of inorganic layered materials, have been the subject of numerous investigations during the last three decades. Interest in layered double metal hydroxides is increasing. They have been widely used as catalysts [15-18], semiconductor materials [19,20], catalyst supports [21], adsorbents [22-24], anion exchangers[25,26], and in medicine. [27,28] Furthermore, LDH materials have been extensively studied in terms of their thermal evolution [29], textural properties [30], formation of nanosized metal particles [31], environmental purpose [32], and photoresponse properties. The structure of the LDHs can be described by $[M^{2+}_{(1-x)}M^{3+}_x(OH)_2]^{x+}[A^{m-}_{x/m}]^{n-}.mH_2O$ formula, where M(II) and M(III) include a variety of bivalent (Mg^{2+}, Zn^{2+}, Co^{2+}, Cu^{2+}, Mn^{2+}) and trivalent (Al^{3+}, Fe^{3+}, Cr^{3+}, V^{3+}, Ga^{3+}, Ti^{3+}) metal ions, A_n^- is an interlayer anion that may be organic and inorganic, such as carboxylate, oxoanions, coordination compounds, and poly-oxometalates, and x generally can have values between 0.1 and 0.33 . [33-35] The thermal treatment of LDHs lead to the collapse of the layered structure and always produce mixed metal oxides (MMOs) which are useful solids and have applications in the areas such as catalysis, lithium-ion batteries, and solar cells because of their superior electrochemical performance. [36] MMO is considered to be a good electrode material for making the dye-sensitized solar cell (DSSC) due to its high purity and good quality control in being manufactured on a large scale. The synthesis methods of LDHs are well-established, and finely dispersed bi- or trimetal oxides can be obtained from the LDHs by calcination because of the uniform distribution of the cations in the brucite layers of LDHs. [37] Another advantage is that LDHs can be also prepared on a large scale.

Among the various semiconducting oxides, ZnO should be an alternative electrode material for DSSCs due to its injection efficiency, band gap (3.37 eV), and electronic properties similar to TiO_2. Moreover, due to the presence of intrinsic impurities, the electron mobility (200–300 $cm^2V^{-1}s^{-1}$) and electron lifetime (>10 s) of ZnO are considerably higher compared to those of TiO_2 (0.1–4.0 $cm^2V^{-1}s^{-1}$), which reduces the electrical resistance and promotes the electron transfer efficiency. [38] Because of having a small specific surface area and reduced dye loading, there are problems when ZnO is used as the semiconductor material. [39] In order to solve these two problems, we propose the synthesis of TiO_2@MMO, which is obtained by the calcined TiO_2@ZnAl-LDH. TiO_2@MMO has a large surface area in comparison with ZnO and the use of TiO_2 in the synthesis of the TiO_2@MMO nanocomposite increases the amount of the adsorbed dye.

In the present work, we used the co-precipitation method in order to combine TiO_2 with the layered double hydroxides. To examine its effect on the performance of the dye sensitized solar cells, the

photovoltaic behaviour of TiO_2@MMO, prepared by calcinations of TiO_2@ZnAl-LDH, was investigated and the results were compared with the data of MMO, which was produced from ZnAl-LDH. It will become a new approach for modifying MMOs in order to obtain the best performance of the photoanode materials.

2. Experimental

2.1 Materials

$Zn(NO_3)_2.6H_2O$, $Al(NO_3)_3.9H_2O$, Na_2CO_3, NaOH, C_2H_5OH, and $TiCl_4$ were purchased from Merck chemical company (Germany). The pH values were adjusted by combining different amounts of 0.2 M solutions of NaOH and 0.1 M solution of Na_2CO_3. N-719 [cis-di(thiocyanato)-N,N–bis(2,2-bipyridyl-4-carboxylicacid-4-tetrabutyl ammonium carboxylate) Ruthenium (II)] was obtained from DyeSol. TiO_2 Degussa P25 TiO_2 (Sigma-Aldrich) nanoparticles around 20 nm, H_2PtCl_6 .$6H_2O$, ethyl cellulose, and terpineol were obtained from Sigma Aldrich. The prepared uniform TiO_2/Zn-Al-LDH paste was coated on FTO (F-doped SnO_2, DyeSol) with the sheet resistance of 15 Ω sq^{-1}. Then, the cells were sealed using syrlyn sheets with 60 µm thickness (DyeSol) and filled with an electrolyte containing 0.5 M lithium iodide, 0.05 M iodine, and 0.4 M 4-tert-butylpyridine in acetonitrile.

2.2 Physical Measurements

Powder X-ray diffraction (PXRD) patterns of the samples were recorded by the Bruker AXS (Germany) model D8 advanced diffractometer for Cu K_α radiation (λ = 1.54 A˚) at 40 kV and 35 mA with Bragg angle ranging from 9 to 70. The FT-IR spectra were obtained using a Bruker (Germany) spectrophotometer in the range of 400–4000 cm^{-1} in the KBr pellets. The thermogravimetric analysis (TGA) was carried out on a Mettler Toledo TGA 851e device (Germany) with the heating rate of 10 °C/min under nitrogen atmosphere. The optical measurements were performed using a UV–vis diffuse reflectance spectrophotometer (Scinco F-4010). The morphology of the obtained products was characterized by scanning electron microscope (SEM, Tescan-Miea3). Photocurrent–voltage (I–V) plots were recorded using a Palmsens potentiostat under the AM1.5 simulated light (Sharif Solar).

2.3 Preparation of TiO_2@ZnAl-LDH

8.91 g (0.03 mol) of Zn $(NO_3)_2.6H_2O$ were dissolved in 50 mL of deionized water in a three-necked round-bottom flask and 5.63 g (0.015 mol) of solution $Al(NO_3)_3.9H_2O$ was added drop-wise to maintain the constant pH at about 9-9.5 with the basic solution (0.67 M Na_2CO_3 and 2.25 M NaOH); then 1.20 gr (0.015 mol) TiO_2 was added. During the whole synthesis process, the obtained reaction mixture was stirred under continuous magnetic stirring in an oil bath for 18 h at 40 °C. The product was centrifuged, thoroughly washed, and dried in an oven at 30 °C.

2.4 Fabrication of DSSC

In the present experiment, a freshly-cleaned transparent FTO conductive glass was used as the electrode. The TiO_2@ZnAl-LDH paste was made from TiO_2@ZnAl-LDH nanostructures, ethyl cellulose, and terpineol in ethanol. The slurry was produced by mixing and grinding 3.0 g of the nanometer sized TiO_2@ZnAl-LDH with ethanol and water in several steps. Then, the grinded slurry was sonicated with the ultrasonic horn and then mixed with the terpineol and ethyl celluloses as the binders. After removing ethanol and water with a rotary-evaporator, the final paste was prepared. The prepared TiO_2@ZnAl-LDH pastes were pasted on FTO using the Doctor Blade technique. Then the electrode was heated at 500 °C for 30 min. After being cooled down to 50 °C, it was immersed into the ruthenium (II) (N-719) (Dyesol) dye solution in ethanol (0.5 mM) and kept at room temperature for 24 h. In order to prepare the counter electrodes, a Pt coated FTO glass electrode was prepared using 0.5 mmol of $H2PtCl_6$.6H2O solution and a drop of this solution was spread on the FTO surface, followed by calcination at 450 °C. Finally, two electrodes were placed together by hot melting the adhesive polymer film at 120 °C. The counter electrode was fully filled with the electrolyte solution (0.5 M lithium iodide, 0.05 M iodine, and 0.4 M 4-tert-butylpyridine in the acetonitrile) through a small hole drilled in it; then, this hole was sealed by a sealing sheet.

3. Results and Discussion

3.1 Characterization of TiO_2@ZnAl-LDH

3.1.1 FT-IR Spectrum

The FT-IR spectra of TiO_2@ZnAl-LDH, before and after calcinations at 500 °C, are shown in Fig. 1. The appearance of the absorption bands at around 3442 cm^{-1} are attributed to the stretching

vibrations of the interlayer water molecules connected to the interlayer carbonate anions. The peak at 1507 cm^{-1} is attributed to the presence of O-C-O. All vibration bands that are detected in the range of 800–400 cm^{-1} are usually assigned to the vibration bands of the M–O and O–M–O groups. The two peaks detected at 552 and 620 cm^{-1} can be attributed to the Ti–O–Ti vibrations of the anatase phase of the TiO_2 crystal. [40] The bands around 427 and 777 cm^{-1} are due to the Al–O and Zn–O lattice vibrations respectively. [15] The sharp intense band observed at 1362 cm^{-1} is assigned to the symmetric and antisymmetric O–C–O stretching vibrations of the monodentate carbonate species [33], that is shown in Fig. 1 (a). Three peaks at 436, 487, and 777 cm^{-1} can be attributed to the stretching mode of Ti-O, Al-O, and Zn-O after calcination (Fig. 1 (b)). The broad band below 980 cm^{-1} in the FT-IR spectra of all the TiO_2 samples belongs to the characteristic vibrations of the inorganic Ti–O–Ti network.[41] The O-C-O asymmetric stretching vibration appears between 1399 and 1541 cm^{-1}. [36,42] The intensity of the CO_3 band disappears after calcination because of decomposition of the CO_3^{2-} groups in the LDH interlayer.

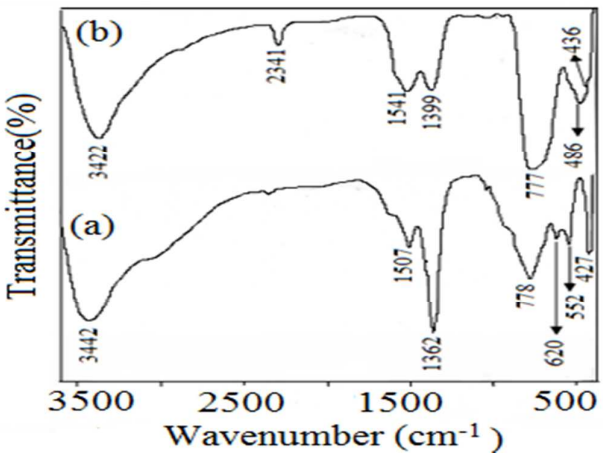

Fig.1. FT-IR spectra of TiO_2/Zn-Al- LDH a) after calcination and b) before calcination at 500°C

3.1.2 X-ray Diffraction Patterns

Fig. 2 illustrates the X-ray diffraction patterns of TiO_2 and TiO_2@ZnAl-LDH before and after calcinations at 500 °C. The XRD pattern in Fig. 2 (a) shows the diffraction pattern of the TiO_2 anatase phase which is matched with the data reported in JCPDS file No. 21-1272. Fig.2 (b) shows the basal peaks of (hkl) planes of (003) and (006) and non-basal peaks of (012), (015), (018), (110), and (113). This XRD pattern shows the formation of ZnAl-LDH which exhibits R3m symmetry and hexagonal lattice with good stacking of the layers. [43] The presence of the TiO_2 anatase phase is confirmed by the (hkl) planes of (101), (200), (105), and (211). After calcination of TiO_2@ZnAl-LDH at 500 °C, the peaks of Zn-Al-LDH were fully disappeared, as can be seen in XRD pattern of Fig. 2 (c). Alternatively, it can be seen that the reflection peaks of ZnO (JCPDS No. 89-1397) appear due to the formation of MMOs containing ZnO. It was also found that Al_2O_3 is the amorphous phase due to the low calcination temperature. The reflection peaks of (101), (105), and (211) show the presence of anatase TiO_2 in TiO_2@ZnAl-LDH after calcination at 500 °C.

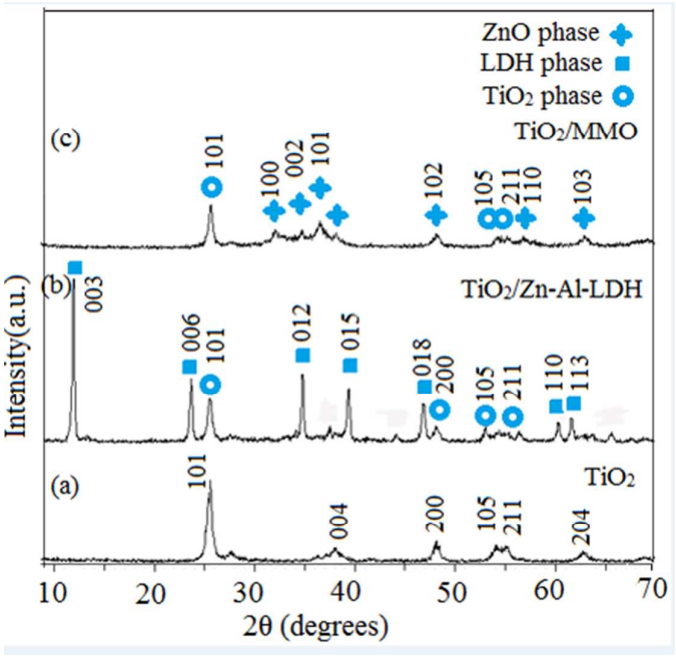

Fig.2. XRD spectra of (a) TiO_2 (b) TiO_2/Zn-Al-LDH (c) TiO_2/MMO

3.1.3 The SEM Images

The surface morphology of the TiO_2@ZnAl-LDH coated electrode was investigated by the SEM image. After calcination at 500°C, the film has TiO_2@MMO plate-like morphology, in which the TiO_2 nanoparticles are placed on the plates, as can be seen in Fig. 3. The thickness of the plates is about 40 nm and their average size is about 300 nm.

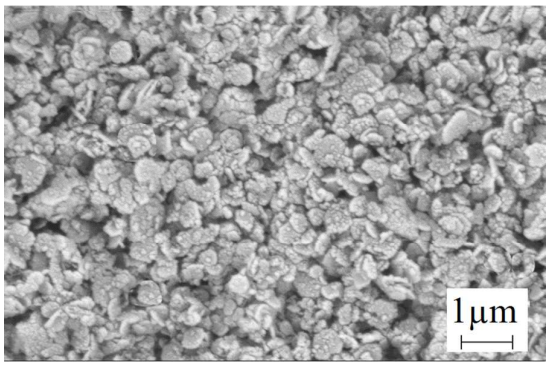

Fig.3. The SEM images of surface morphology electrode based on TiO_2/Zn-Al LDH after calcination at 500°C

3.1.4 The Cross-Section SEM Images

The cross-sectional SEM image in Fig. 4 shows that the film-thickness on the FTO substrate was nearly 4.7 μm after calcination at 500 °C. TiO_2@MMO was coated on FTO substrates without any noticeable disorder. The surface of the film is smooth with very little vacancies and no cracks are observed on the film due to the nanosize plates.

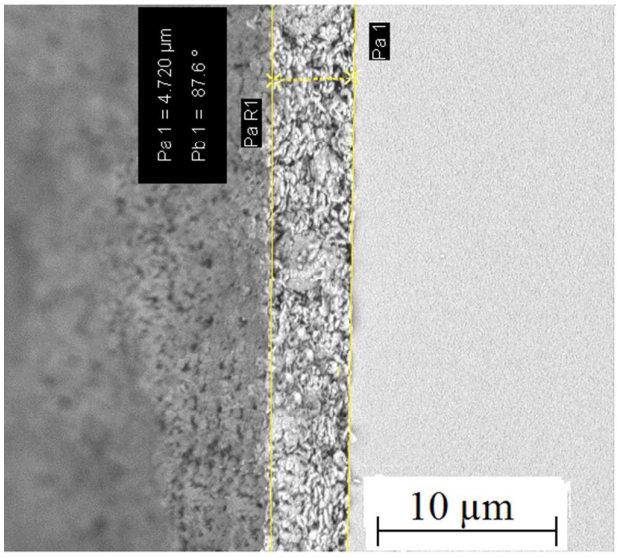

Fig.4. The cross section of the SEM images as-prepared TiO2/Zn-Al- LDH photoanod after calcination at 500 °C

3.1.5 Electron X-ray Diffraction Spectroscopy (EDX)

The chemical compositions of TiO_2@MMO after calcination at 500 °C are presented in Fig. 5. The EDX analysis shows that the peaks associated with Ti, Zn, Al, and O are clearly observed and provide strong evidence that the nanocrystals are composed just from TiO_2@MMO.

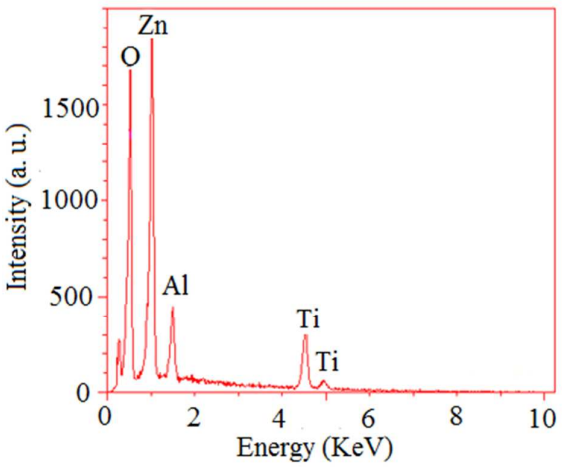

Fig.5. EDX pattern of TiO2/ MMO nanocomposite

3.1.6 TGA Analysis

The results of the thermal analysis of the materials are presented in TGA and DTG curves of TiO_2@ZnAl-LDH (Fig. 6). Two weight losses are observed: the first one is in the range of room temperature to 200 °C, due to the evaporation of water from the surface and the interlayers of LDH; the second weight loss at higher temperatures (200–390 °C) is attributed to the dehydroxylation of the brucite-like layers, corresponding to the mass loss process. [19] The DTG curve shows two distinct peaks. The first peak appeared at 170 °C is attributed to the removal of water and the second peak at 250 °C corresponds to decomposition of the carbonate ions in the interlayers of LDH.

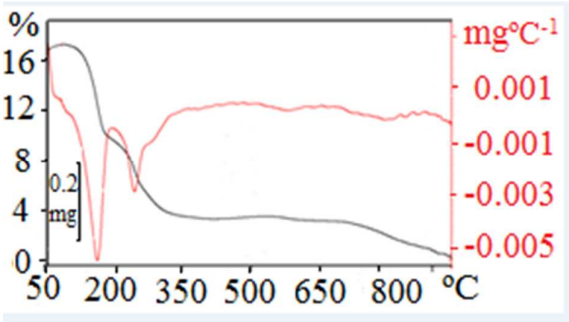

Fig. 6. TGA and DTG curves of TiO2/Zn-Al- LDH

3.2 Optical Studies

The UV–vis diffuse reflectance (DRS) spectrum of the calcined TiO_2@LDHs without dye sensitization is presented in Fig. 7. DRS is used to determine the band gap energy. Using the absorption data, the band gap was estimated by the Tauc's relationship:

$$\alpha = \frac{a_0(h\upsilon - Eg)^n}{h\upsilon} \quad (1)$$

where α is the absorption coefficient, hυ is the photon energy, α_0 and h are the constants, E_g is the optical band gap of the material, and n depends on the type of electronic transition and can be any value between ½ and 3. [44] The energy gap of the film was determined by extrapolating the linear portion of the plots of $(\alpha h\upsilon)^2$ against hυ to the energy axis. The calcined TiO_2@ZnAl-LDH exhibited a band gap of 3.3 eV, so the TiO_2@MMO nanocomposite has low absorbance in the visible area of the solar spectrum. This leads to strongly weakening the degradation performance, related to the photocatalytic activity of the TiO_2@MMO nanocomposite on N719 dye, under the visible area of the solar light. [45]

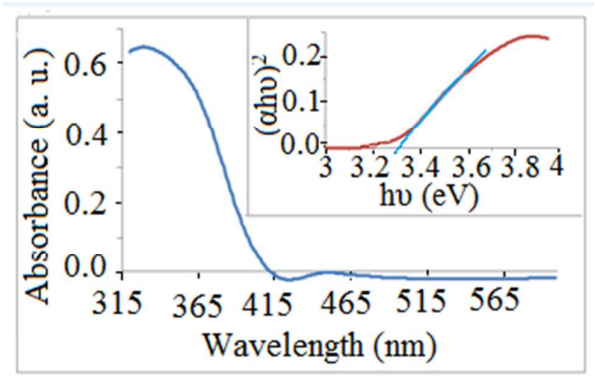

Fig.7. UV–vis diffuse reflectance spectra of TiO_2/MMO

3.3 DSSCs Performance

As equation (2) shows, the whole solar to electrical energy conversion efficiency, η , for a solar cell is given by the photocurrent density measured at short circuit (J_{sc}), the open circuit photovoltage (V_{oc}), the fill factor of the cell (FF), and the power of the incident light (P_{in}):

$$\eta = \left(\frac{J_{SC} * V_{OC} * FF}{P_{in}}\right) \quad (2)$$

The fill factor can accept values between 0 and less than 1 and is defined by the ratio of the full power (P_{max}) of the solar cell per unit area divided by (V_{oc}) and (J_{sc}) according to equation (3):

$$FF = \left(\frac{P\ max}{J_{SC} * V_{OC}}\right) \quad (3)$$

The full power is achieved as the product of the photocurrent and photovoltage at the voltage where the power output of the cell is maximum. [46]

In order to study the performance of fabricated DSSC, the current–voltage (I–V) curves are shown in Fig. 8. The calculated η value is 1.51% with short circuit current density (J_{sc}) of 2.63 mA/cm^2, open circuit voltage (V_{oc}) of 0.81 V, and a fill factor of 0.7.

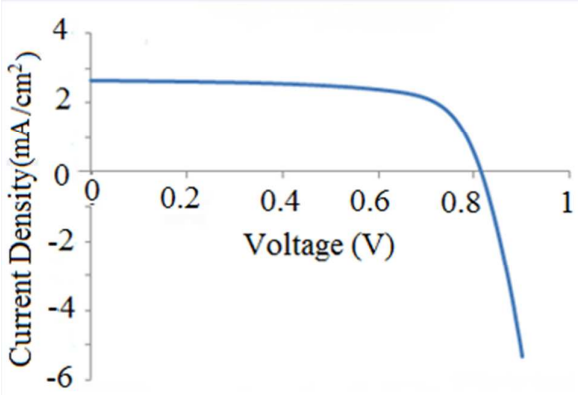

Fig.8. Current density versus voltage (J- V) curves for TiO_2/MMO

Based on the research published by Jianqiang et al. , MMOs resulted from the calcination of ZnAl-LDH with the Zn–Al molar ratio of 3:1 exhibited a band gap of 3.13 ev and plate-like structure with the thickness of 150 nm and average size of 1 µm. The thickness of the MMO film that was used as the photoanode was about 8.6 µm. When this film was applied as the photoanode, the best efficiency was 0.0129% with J_{sc} of 0.073 mA/cm^2, V_{oc} of 0.43 V, and fill factor of 0.41. [37]

Table 1 shows a comparison of the photovoltaic parameters of DSSC, obtained from the calcination of ZnAl-LDH with the Zn:Al molar ratio of 3:1 by Jianqiang et al. [37], with TiO_2@MMO derived from TiO_2@ZnAl-LDH (the present study).

RSC Advances

ARTICLE

Table 1. Current–voltage characteristics of DSSCs based on TiO_2@MMO

Sample	Photoanode thickness (μm)	J_{sc} (mA/cm^2)	V_{oc} (V)	FF	η (%)	Refs.
TiO_2@ZnAl-LDH	4.7	2.63	0.81	0.70	1.50	This study
TiO_2	5.3	10.32	0.68	0.64	4.50	This study
ZnAl-LDH	8.6	0.073	0.43	0.41	0.01	[37]
ZnO nanowire	-	1.57	0.67	0.30	0.32	[48]

Based on our results, it is observed that by adding TiO_2 to ZnAl-LDH (mol ratio of TiO_2:Zn = 0.5) and calcinating it at 500°C, the conversion efficiency increases to 1.5% when the active area was 0.25 cm^2.

This improved conversion efficiency can be assigned to the increased surface area of the TiO_2@MMO film.

Comparing the aforementioned research [37] with this study shows the following differences: the electrode based on the MMO derived from Zn-Al-LDH had thickness of about 150 nm, the average size of 1 μm, and plate-like nanoparticles; while in the present study, the average thickness of the film and the average size of the nanoparticles decreased to about 40 nm and 300 nm respectively, which leads to the smoothness and homogeneousness of the film and decrease in the vacancies within the film.

The easier preparation, lower thickness, and higher efficiency of TiO_2@MMO nanocomposite are the advantages of the present study in comparison with those of ZnAl-LDH reported by Jianqiang et al. [37]

Addition of TiO_2 into MMO increases the ban d gap energy to 3.3 ev. Therefore, TiO_2@MMO had higher Fermi level potential than MMO which resulted in increasing V_{OC} of TiO_2@MMO. Then, improvement of V_{oc} from 0.43 V (Jianqiang et al.[37]) to 0.81 V can be due to the shift of conduction band to more negative values after the surface modification of MMO by TiO_2. Based on the literature, high thickness and crack sites decrease the open circuit voltage. The decrease in open circuit voltage can be explained by lower diffusion of electrolyte species (electron life time) and higher chance of recombination.[47]

It is important to mention that decrease in the thickness of the TiO_2@MMO layer (about 4.76 μm) is the other reason for increase in V_{oc} in the present study in comparison with ref -37.

Scheme 1 presents the energy band diagram of TiO_2@MMO. TiO_2@MMO forms localized acceptor levels in the forbidden band gap which leads to decrease in the transportation resistance. The higher J_{sc} for the TiO_2@MMO sample than MMO is attributed to much lower electron transportation resistance and electron recombination reaction at anode/electrolyte.

Electrons which are injected from the dye to TiO_2 and further to MMO have fewer chances of recombination with the electrolyte because of the energy barrier which is created between TiO_2 and MMO there upon improved V_{oc} to 0.81 V at TiO_2@MMO. Beside, MMO naturally block recombination electron and hole that improved V_{OC}.

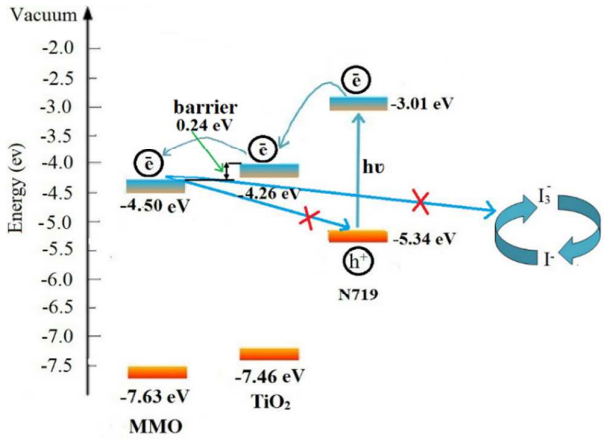

Scheme 1. Energy band diagram of TiO_2/MMO and N719

4. Conclusions

In summary**,** TiO_2@MMO nanocomposite derived from TiO_2@ZnAl-LDH was used as the photoelectrode material for the dye-sensitized solar cells, and the photovoltaic performance of these nanoparticles was investigated. Addition of TiO_2 to ZnAl-LDH had slight effect on the E_g value but led to considerable improvement of the DSSC performance of the final products. It was also realized that the morphology of the prepared TiO_2@MMO, the size of the nanolayers, and the film thickness on FTO are beneficial for the photovoltaic performance.

The TiO_2@ZnAl-LDH based solar cell sensitized with the N719 dye showed maximum conversion efficiency of 1.5%. Thus TiO_2@MMO nanocomposite improved open circuit voltage and efficiency of DSSCs by using lower thickness of the photoanode. The easier preparation, lower thickness, and higher efficiency of TiO_2@MMO nanocomposite are the advantages of the present study in comparison with those of ZnAl-LDH reported by Jianqiang et al [29]

Acknowledgements

We are grateful to Azarbijan Shahid Madani University for financial supports.

Notes and references

1 L.-F. Lai, C.-L. Ho, Y.-C. Chen, W.-J. Wu, F.-R. Dai, C.-H. Chui, S.-P. Huang, K.-P. Guo, J.-T. s. Lin, H. Tian, S.-H. Yang and W.-Y. Wong, *Dyes Pigm.*, 2013, **96**, 516-524.

2 H. Tributsch and M. Calvin, *J. Photochem. Photobiol.,* 1971, **14**, 95-112.

3 G. D. Sharma, G. E. Zervaki, P. A. Angaridis, A. Vatikioti, K. S. V. Gupta, T. Gayathri, P. Nagarjuna, S. P. Singh, M. Chandrasekharam, A. Banthiya, K. Bhanuprakash, A. Petrou and A. G. Coutsolelos, *Org. Electron.,* 2014, **15**, 1324-1337.

4 H. J. Jo, J. E. Nam, D.-H. Kim, H. Kim and J.-K. Kang, *Dyes Pigm.*, 2014, **102**, 285-292.

5 B. O'Regan and M. Gratzel, *Nature*, 1991, **353**, 737-740.

6 M. Gratzel, *Nature*, 2001, **414**, 338-344.

7 B. Hu, Q. Tang, B. He, L. Lin and H. Chen, *J. Power Sources,* 2014,**267**, 445-451.

8 Y. Duan, Q. Tang, Z. Chen, B. He and H. Chen, *J. Mater. Chem. A,* 2014, **2**, 12459-12465.

9 Z. Wang, Q. Tang, B. He, H. Chen and L. Yu, *Electrochimica Acta*, 2015, **178**, 18-24.

10 Z. Wang, Q. Tang, B. He, X. Chen, H. Chen and L. Yu, *J. Power Sources,* 2015, **275**, 175-180.

11 F. Bella, A. Sacco, G. Massaglia, A. Chiodoni, C. F. Pirri and M. Quaglio*, Nanoscale*, 2015, **7**, 12010-12017.

12 Y.-Fen Wang, X.-Fei Li, D.-Jun Li, Y.-Wei Sun and X.- Xi Zhang, *J. Power Sources,* 2015,**280**, 476-482.

13 D. Pugliese, A. Lamberti, F. Bella, A. Sacco, S. Bianco and E. Tresso*, Organic Electronics,* 2014,**15(12)**, 3715-3722.

14 J. Luo, J.- H. Im, M. T. Mayer, M. Schreier, M. K. Nazeeruddin, N.- G. Park, S. D. Tilley, H. J. Fan and M. Grätzel, Science, 2014, **345(6204)**, 1593-1596.

15 K. M. Parida, M. Sahoo and S. Singha, *J.Catal.*, 2010, **276**, 161-169.

16 B. M. Choudary, T. Someshwar, M. Lakshmi Kantam and C. Venkat Reddy, *Catal. Commun.,* 2004, **5**, 215-219.

17 S. Kerchiche, R. Chebout, A. Barama and K. Bachari, *Arabian J. Chem.*; doi:10.1016/j.arabjc.2012.08.005.

18 S. Kühl, J. Schumann, I. Kasatkin, M. Hävecker, R. Schlögl and M. Behrens, *Catal. Today*, doi:10.1016/-j.cattod.2014.08.029

19 X. Wang, P. Wu, Z. Huang, N. Zhu, J. Wu, P. Li and Z. Dang, *Appl. Clay Sci.,* 2014, **95**, 95-103.

20 S.-J. Xia, F.-X. Liu, Z.-M. Ni, W. Shi, J.-L. Xue and P.-P. Qian, Appl. Catal., B*: Environmental*, 2014, **144**, 570-579.

21 F.-A. He and L.-M. Zhang, *J. Colloid Interface Sci.,* 2007, **315**, 439-444.

22 Y.-M. Zheng, N. Li and W.-D. Zhang, *Colloids Surf., A,* 2012, **415**, 195-201.

23 F. Khodam, Z. Rezvani and A. R. Amani-Ghadim, J. Ind. Eng. Chem., 2015, **21**, 1286-1294.

24 T. Türk, İ. Alp and H. Deveci, *J. Hazard. Mater.,* 2009, **171**, 665-670.

25 K. Muramatsu, O. Saber and H. Tagaya, *J. Porous Mater.,* 2007 **14**, 481-484.

26 A. Fraccarollo, M. Cossi and L. Marchese, *Chem. Phys. Lett.,* 2010, **494**, 274-278.

27 R. Xiao, W. Wang, L. Pan, R. Zhu, Y. Yu, H. Li, H. Liu and S.-L. Wang, *Mater. Sci. Eng., B*, 2011, **46**, 2635–2643.

28 S. Bhattacharyya, R. A. Kudgus, R. Bhattacharya and P. Mukherjee, *Pharm. research*, 2011, **28**, 237–259.

29 H. Zhu, L. Wang, P. Tang, Y. Feng and D. Li, *Particuology*, 2012, **10**, 503-508.

30 O. Saber and H. Tagaya, *Mater. Chem. Phys.,* 2008, **108**, 449-455.
31 E. M. Seftel, E. Popovici, M. Mertens, E. A. Stefaniak, R. Van Grieken, P. Cool and E. F. Vansant, *Appl. Catal., B,* 2008, **84**, 699-705.
32 D. Chen, Y. Li, J. Zhang, W. Li, J. Zhou, L. Shao and G. Qian, *J. Hazard. Mater.,* 2012, **243**, 152-160.
33 R. K. Sahu, B. S. Mohanta and N. N. Das, J. Phys. Chem. Solids, 2013, **74**, 1263-1270.
34 K. M. Parida and L. Mohapatra, *Chem. Eng. J.,* 2012, **179**, 131-139.
35 C. Manzi-Nshuti, D. Chen, S. Su and C. A. Wilkie, *Polym. Degrad. Stab.,* 2009, **94**, 1290-1297.
36 J. Song, M. Leng, X. Fu and J. Liu, *J. Alloys Compd.,* 2012, **543**, 142-146.
37 L. Zhang, J. Liu, H. Xiao, D. Liu, Y. Qin, H. Wu, H. Li, N. Du and W. Hou, *Chem. Eng. J.,* 2014, **250**, 1-5.
38 S. G. Kumar and K. S. R. K. Rao, *RSC Adv.,* 2015, **5**, 3306-3351.
39 X. Fang, Y. Li, S. Zhang, L. Bai, N. Yuan and J. Ding, *Sol. Energy*, 2014, **105**, 14-19.
40 M. Hadnadjev-Kostic, T. Vulic and R. Marinkovic-Neducin, *Adv. Powder Technol.,* 2014, **25**, 1624-1633.
41 N. Mir and M. Salavati-Niasari, *Mater. Res. Bull.,* 2013, **48**, 1660-1667.
42 X. Fan, Z. Yang, X. Xie, W. Long, R. Wang and Z. Hou, *J. Power Sources*, 2013, **241**, 404-409.
43 Y. Sun, Y. Zhou, Z. Wang and X. Ye, *Appl. Surf. Sci.,* 2009, **255**, 6372-6377.
44 N. Mir and M. Salavati-Niasari, *Electrochim. Acta*, 2013, **102**, 274-281.
45 S. Yuan, Q. Tang, B. He, L. Men and H. Chen, *Electrochim. Acta*, 2014, **125**, 646-651.
46 M. Dadkhah and M. Salavati-Niasari, *Electrochim. Acta*, 2014, **129**, 62-68.
47 M. R. Golobostanfard and H. Abdizadeh, Sol. Energy Mater. Sol. Cells, 2014, **120, Part A**, 295-302.
48 M. Zi, M. Zhu, L. Chen, H. Wei, X. Yang, B. Cao, Ceramics International, 2014, 40, 7965–7970

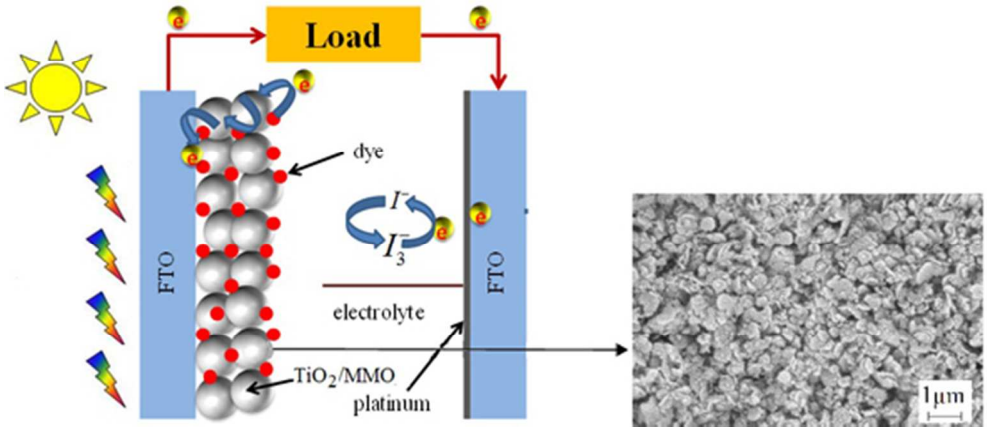

158x72mm (96 x 96 DPI)